Dalton Transactions



COMMUNICATION

View Article Online
View Journal | View Issue



Cite this: *Dalton Trans.*, 2023, **52**, 5034

Received 27th March 2023, Accepted 30th March 2023 DOI: 10.1039/d3dt00932q

rsc.li/dalton



Bingqing Liu, (D) Yasmine S. Zubi (D) and Jared C. Lewis (D)*

Artificial metalloenzymes (ArMs) can combine the unique features of both metal complexes and enzymes by incorporating a cofactor within a protein scaffold. Herein, we describe a panel of ArMs constructed by covalently linking Ir(III) polypyridyl complexes into a prolyl oligopeptidase scaffold. Spectroscopic methods were used to examine how properties of the resulting ArMs are influenced by structural variation of the cyclometalated ligands and the protein scaffold. Visible light photocatalysis by these hybrid catalysts was also examined, leading to the finding that they catalyze inter/intramolecular [2 + 2] photocycloaddition in aqueous solution. Low but reproducible enantioselectivity was observed using a cofactor that undergoes partial kinetic resolution upon bioconjugation within the ArM active site, showing the importance of scaffold/cofactor interactions for enabling selective ArM photocatalysis. Further evidence of the importance of cofactor/scaffold interactions was provided by analyzing native POP peptidase catalysis by the ArMs. Together, these studies show how Ir(III)-based ArMs constitute a promising starting point for ongoing studies to control the stereoselectivity of EnT reactions by engineering substrate binding/activation motifs in POP.

Visible light photocatalysis provides facile access to reactive radical and diradical intermediates that enable a range of useful synthetic transformations *via* electron transfer (ET) or energy transfer (EnT).^{1,2} Transition metal polypyridyl complexes have received increasing attention based on their remarkable photophysical properties, including high photostability, strong absorption of visible light, and high excited-state quantum yields.³ Both tris-(2-phenylpyridine) (Ppy₃) and heteroleptic bis-(2-phenylpyridine) bipyridine (Ppy₂Bpy) Ir(III) complexes have been employed as photocatalysts for cycloaddition and cyclization reactions involving a broad range of

Department of Chemistry, Indiana University, Bloomington, Indiana 47405, USA. E-mail: jcl3@iu.edu

substrates.⁴ These photocatalysts have been used in combination with chiral Brønsted acid co-catalysts to enable enantioselective [2 + 2] photocycloadditions at cryogenic temperatures.^{5,6} Very recently, two groups independently established that a benzophenone photosensitizer could be genetically encoded into different protein scaffolds to enable similar reactions with high selectivity imposed by second sphere interactions.^{7,8}

Based on these precedents, we hypothesized that a protein scaffold could be used to control the photophysical and catalytic properties of robust Ir(III) polypyridyl photocatalysts in analogy to reports using other protein-encapsulated chromophores. 9-13 We recently established that artificial metalloenzyme (ArM) photocatalysts could be constructed by covalently linking tris-bipyridine Ru(II) complexes within the large active site of a prolyl oligopeptidase (POP) from Pyrococcus furiosus. 14,15 These ArMs afforded higher yields and rates for the [2 + 2] photocycloaddition of dienones than $Ru(bpy)_3^{2+}$, indicating that the POP scaffolds could be an effective platform to enhance the reactivity of photocatalysts. Incorporating Ir(III) complexes within POP would significantly expand the range of processes that could be achieved using this platform. These complexes possess a range of triplet excited state levels that can be applied for energy transfer to a broad scope of substrates, and their unique structures would enable further interrogation of second sphere effects on the photophysical properties of the embedded metal complexes.¹⁶

In this study, we report a panel of Ir(III)Ppy₂Bpy cofactors (1–5) featuring varied Ppy ligands and an *exo*-bicyclo[6.1.0] nonyne (BCN)-substituted bipyridine ligand (Fig. 1a). Introducing electron-withdrawing groups or benzannulation onto parent complex 3 can be used to tune the energy of the HOMO in these cofactors for different reactions.¹⁷ Moreover, the variable sizes of these ligands allow for analysis of scaffold/cofactor/substrate interactions independent of ArM activity (*vide infra*). The L-4-azido-phenylalanine (AzF or Z) was genetically encoded at site 53 of POP (POP-Z53) and used to covalently link cofactors 1–5 *via* strain-promoted azide–alkyne

[†]Electronic supplementary information (ESI) available: Supplemental figures, detailed procedures and results for all reported experiments, and data for compound characterization. See DOI: https://doi.org/10.1039/d3dt00932g

Dalton Transactions Communication

Fig. 1 (a) Chemical structures of Ir(III) cofactors 1-5 and scheme for the formation of POP-Z53-1-5; (b) Schemes for visible-light-induced photocycloaddition reactions catalyzed by Ir(III)-ArMs.

cycloaddition (SPAAC) to form the corresponding ArMs (POP-Z53-1-5) (Fig. 1a). The photophysical properties of these ArMs were characterized, their photocatalytic activity toward inter- and intramolecular [2 + 2] cycloadditions reactions was evaluated, and their ability to catalyze peptide hydrolysis, the native activity of the POP scaffold, was analyzed.

Cofactors 1–5 were synthesized by first treating the respective Ppy ligand with IrCl₃·3H₂O, reacting the resulting [(Ppy)₂IrCl]₂ complexes with 4-hydroxymethyl-Bpy, and reacting the resulting (Ppy)₂Ir(Bpy) complexes with PNP-BCN. 19 A POP variant with a M53Z mutation (POP-Z53) was expressed in E. coli with a yield of ~100 mg L⁻¹ and confirmed by intact electrospray ionization mass spectrometry (ESI-MS) (Fig. S1 and S2†).20 Subsequently, bioconjugation of 1-5 to POP-Z53 was accomplished to afford POP-Z53-1-5, formation of which was verified by intact ESI-MS (Table S1, Fig. S1†). All reactions were complete in 5 minutes except for those with cofactor 5, perhaps due to its relatively large size compared to the other complexes.

The UV-vis absorption spectra of complexes 1-5 and POP-Z53-1-5 were next examined in aqueous solution. A representative spectrum for POP-Z53-3 is shown in Fig. 2a, the collected spectra are presented in Fig. S3,† and the absorption band maxima and molar extinction coefficients are tabulated in Table S1.† The intense absorption bands ($\varepsilon \ge 10^4 \text{ L mol}^{-1}$ cm^{-1}) at wavelengths of 250–360 nm in POP-Z53-1-3, 250-380 nm in POP-Z53-4, and 250-460 nm in POP-Z53-5 can be predominantly assigned to ligand-localized spin-allowed

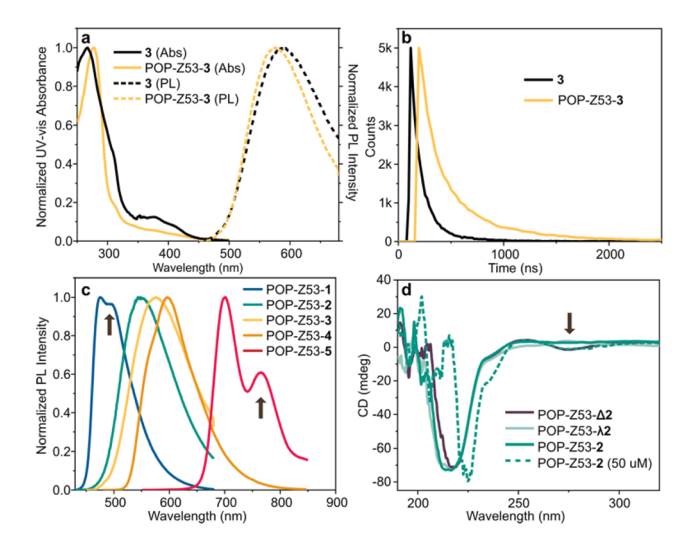


Fig. 2 (a) Normalized UV-vis absorption and photoluminescence (PL) spectra and (b) PL decay characteristics of 3 (50 µM) in 10% CH₃CN/H₂O and POP-Z53-3 (50 µM) in H₂O at room temperature. (c) Emission spectra of POP-Z53-1-5 (50 μ M) in H₂O at room temperature. (d) Circular dichroism spectra of POP-Z53-2 ($\Delta/\Lambda/\text{rac}$) in agueous solution (10 or 50 uM).

 $^{1}\pi$, π^{*} transitions. $^{21-23}$ The broader and weaker bands at 360-500 nm in POP-Z53-1-3, 380-530 nm in POP-Z53-4, and 460-620 nm in POP-Z53-5 likely originate from charge transfer (CT) transitions, which are also observed in the spectra of the corresponding cofactors (Fig. S3-S5†).

Since Ir(III) complexes typically exhibit phosphorescence originating from triplet excited states, photoluminescence spectra of 1-5 and the corresponding ArMs were also collected to interrogate their triplet excited-state properties (Fig. 2a, Fig. S6, and Table S1†). While POP-Z53-1, -4, and -5, displayed similar emission properties as the corresponding cofactors, blue-shifted emissions were observed for POP-Z53-2 and -3, indicating that the excited state of these cofactors was being influenced by the POP scaffold. Additionally, the luminescence featured long lifetimes ranging from hundreds of nanoseconds to several microseconds and was readily quenched by oxygen, which confirms the phosphorescent nature of these bands emanated from the triplet excited states of Ir(III) cofactors (Fig. 2b, Fig. S7†). The emission spectra of POP-Z53-1 and POP-Z53-5 displayed vibronic structures with long-lived lifetimes of several microseconds, suggesting the emissions can be predominantly assigned to the ligand-localized $^3\pi,\pi^*$ state (Fig. 2c, arrows).²¹ By contrast, POP-Z53-2 and POP-Z53-3 exhibited broad and featureless emission bands with moderate lifetimes of several hundred nanoseconds. These features are typical ³CT (³MLCT/³LLCT) transitions partially mixed with $^{3}\pi,\pi^{*}$ character. Of particular note, the lifetimes of POP-Z53-1-5 have increased by ca. 100-1000 nanoseconds compared to the corresponding cofactors 1-5, which is consistent with our previously reported Ru(II) ArMs (Fig. 2c and Fig. S7†). Additionally, triplet excited state energies (E_T) based on the onset of their emissions were calculated (Table S1†). Slightly

Communication Dalton Transactions

higher $E_{\rm T}$ values were observed for ${\rm Ir}(m)$ ArMs when compared with 1–5. The amplification in both lifetimes and $E_{\rm T}$ can be attributed to the hydrophobic environment within the POP scaffold.²⁴

The interaction between the cofactor and protein scaffold was further examined by using circular dichroism (CD) spectroscopy. Nearly identical CD spectra were obtained for both POP and POP-Z53-1-5, suggesting the incorporation with cofactors exerts a negligible effect on secondary structures of proteins (Fig. S8†).²⁵ Notably, Cotton effects at 250-300 nm were observed for POP-Z53-2 (Fig. 2d). To confirm which cofactor enantiomer was being resolved to elicit this effect, optically-active cofactors Δ - and Λ -2 were prepared and linked to POP-Z53 to afford POP-Z53- (Δ/Λ) 2. The CD spectrum of POP-Z53-2 is reminiscent of POP-Z53-Δ2, suggesting that the chiral Ir(III) complex undergoes kinetic resolution during bioconjugation within the POP scaffold. A similar phenomenon was also observed for Ru(II) ArMs in our previous study. 14,26,27 The CD spectra for POP-Z53-1-5 acquired at 20-100 °C were essentially identical, suggesting that cofactor incorporation does not significantly reduce the high stability of the POP scaffold (Fig. S8†).

While spectroscopic data provided evidence for encapsulation of 1-5 within the POP active site, we hypothesized that the native peptidase activity of POP could be used to obtain further evidence for this important aspect of ArM structure. POP family enzymes are unique among serine proteases in that their hydrolase domain is capped by a β-propeller domain that regulates substrate access to their active site.²⁸ Moreover, MD simulations indicate that domain closing brings His592, which is part of the catalytic triad of this enzyme along with Ser477 and Asp560, into a catalytically competent orientation.²⁹ Because Z-53 is distal to the catalytic triad residues, we reasoned that the ArMs generated in this study would retain catalytic activity if the enzyme could adopt a closed conformation with the cofactor fully encapsulated.³⁰ If the cofactor projected out of the enzyme and thereby blocked domain closing, however, catalysis should be completely inhibited. Formation of p-nitroaniline (pNA) from hydrolysis of benzyloxycarbonyl-alanyl-prolyl-p-nitroanilide (Z-Ala-Pro-pNA) monitored by UV-vis spectroscopy (Fig. 3a), and steady state kinetic parameters were obtained (Table S2†). POP-Z53-2 and POP-Z53-5 were selected for analysis due to the large size difference in their respective cofactors. Both ArMs displayed a 3.3-fold decrease in enzymatic activity compared to apo POP, suggesting that the cofactors are covalently bound and that they alter substrate binding but still allow the enzyme to adopt a closed conformation with the cofactor completely encapsulated. In a complementary experiment aimed at better distinguishing the sizes of cofactors 2 and 5, we also investigated Z-Ala-Pro-pNA hydrolysis in the presence of 10 or 100 equiv. of (S)-1-Boc-2-cyanopyrrolidine, which is a known covalent inhibitor of POP (Fig. 3b-d).31 In this experiment, two-fold higher inhibition was observed for POP-Z53-5 relative to POP-Z53-2. Because both ArMs have the same activity in the absence of inhibitor (and can therefore access the required closed form of

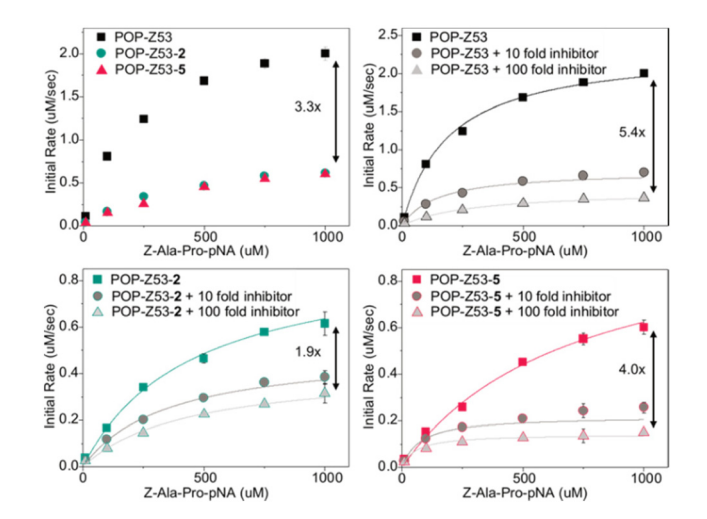
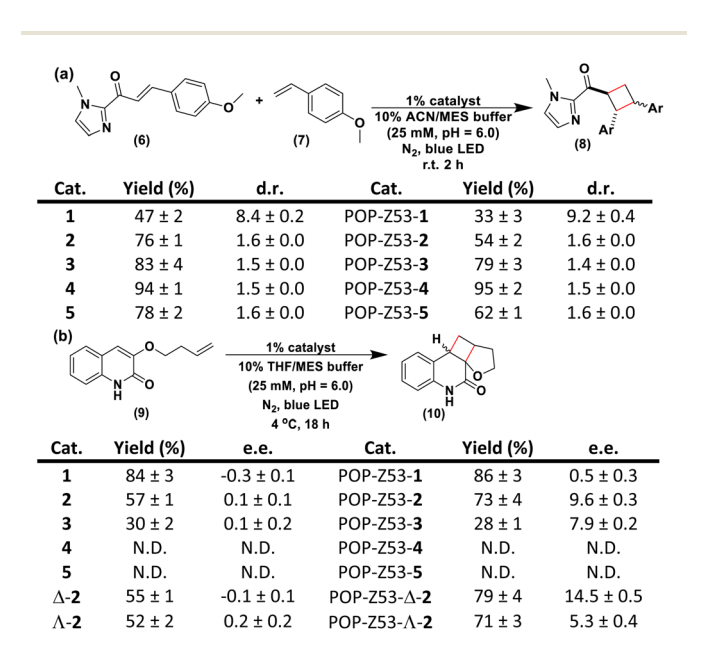


Fig. 3 Kinetic analysis for the hydrolysis of Z-Ala-Pro-pNA by POP-Z53/POP-Z53-2/POP-Z53-5 (10 nM) at 85 °C with or without different amounts of (S)-1-Boc-2-cyanopyrrolidine. Using the Michaelis–Menten equation, a plot of initial rates (μ M/sec) versus the substrate concentration (μ M) was fitted.

the enzyme), this result suggests that the larger size of 5 causes greater steric crowding within the active site that leads to greater sensitivity to the inhibitor.

Finally, ArM photocatalysis was investigated in aqueous solution using inter- and intra-molecular [2 + 2] cycloaddition model reactions (Scheme 1, Table S3-9†). 32,33 All ArMs were



Scheme 1 (a) Intermolecular [2 + 2] photocycloaddition of cinnamoyl imidazole (6) and 4-methoxy styrene (7). (b) Intramolecular [2 + 2] photocycloaddition of 3-(3-buten-1-yloxy)-2(1H)-quinolinone (9). Yields and diastereomer ratios (d.r.) were determined by UHPLC analysis using 1,3,5-trimethoxybenzene (TMB) or phenol as an internal standard. Reactions were performed in triplicate and are reported as averages with standard deviations. Enantiomeric excess was determined by using chiral ultra-performance liquid chromatography (UPLC) analysis.

Dalton Transactions Communication

active toward both reactions, with POP-Z53-4 and -1 providing the highest yields for the inter- and intramolecular reactions, respectively. This difference reflects the established need to match the triplet energy of the Ir(III) cofactor with the triplet state of the substrate. The yield of 8 dropped only slightly (from 94 \pm 2 to 89 \pm 2, Table S6†) when the ArM loading was reduced to 0.1 mol% while the yield for the cofactor alone dropped to 66 \pm 3 (Table S6†). The yield of 10 using both the ArM and free cofactor decreased to roughly 18% upon a similar reduction in catalyst loading (Table S7†).

The observed diastereoselectivities for intermolecular [2+2] photocycloaddition were similar to those obtained for the cofactors alone, but POP-Z53-2 catalyzes intramolecular [2+2] photoreaction of **9** to afford **10** with 9.6 \pm 0.3% e.e. at 4 °C. As noted above, **2** is the only cofactor evaluated that appears to undergo partial resolution upon bioconjugation to POP, suggesting that it can bind in a selective fashion within the active site. This selective binding appears to translate to improved photocatalysis selectivity since POP-Z53- Δ -2 provides **10** with an improved 14.5 \pm 0.5% e.e. while the Δ -enantiomer provides only 5.3 \pm 0.4% e.e. Negligible enantioselectivity was observed for Ir(III) ArMs linked at other sites in the POP scaffold (Table S9†), showing that cofactor structure, chirality, and linkage site are critical for stereoselective photocatalysis.

In this study, a series of clickable Ir(III) complexes were covalently incorporated into a POP scaffold to form ArM photocatalysts. Prolonged triplet lifetimes of these Ir(III) cofactors result from incorporation into POP. The POP scaffold enables partial kinetic resolution of racemic complex 2 to enrich the Δ -2 enantiomer in the ArM, indicating that secondary interactions between POP and the chiral Ir fragment can occur. Analysis of native POP peptidase catalysis using the Ir(III) ArMs provides further evidence that the cofactor can be fully encapsulated within POP and suggests that crowding by the bulky cofactors restricts substrate access within the active site. The ArMs also catalyze both intermolecular and intramolecular EnT-induced photocatalysis. Importantly, the ArM generated from cofactor 2 provides a low but reproducible 9.6% e.e., and using Δ -2 improves this to 14.5% e.e., highlighting the importance of scaffold/cofactor interactions in enabling selective ArM photocatalysis. These studies show how Ir(III)-based ArMs constitute a promising starting point for ongoing efforts to control the stereoselectivity of EnT reactions by engineering substrate binding/activation motifs into the POP active site.

Conflicts of interest

There are no conflicts to declare.

Acknowledgements

This study was supported by the U.S. Army Research Laboratory and the U.S. Army Research Office under Contract/Grant W911NF-22-1-0118 and by the NSF (CHE-2154726). Y.S.Z

gratefully acknowledges receipt of a predoctoral fellowship from the Graduate Training Program in Quantitative and Chemical Biology at Indiana University (T32 GM131994) and the IUB Chester Davis Fellowship in Inorganic Chemistry. NMR data were acquired on a spectrometer funded by the NSF (MRI CHE-1920026) using a Prodigy probe that was partially funded by the Indiana Clinical and Translational Sciences Institute. We thank Dr Jonathan Trinidad for assistance with intact protein ESI-MS; Dr Giovanni Gonzalez-Gutierrez for assistance with various instrumentation in the IU Physical Biochemistry Instrumentation Facility and for allowing us to borrow a low-volume cuvette for luminescence measurements; and Prof. Amar Flood for access to a UV-Vis spectrophotometer and a fluorometer.

References

- 1 J. Großkopf, T. Kratz, T. Rigotti and T. Bach, *Chem. Rev.*, 2022, **122**, 1626.
- 2 F. Strieth-Kalthoff, M. J. James, M. Teders, L. Pitzer and F. Glorius, Chem. Soc. Rev., 2018, 47, 7190.
- 3 M. H. Shaw, J. Twilton and D. W. C. MacMillan, J. Org. Chem., 2016, 81, 6898.
- 4 J. Twilton, C. C. Le, P. Zhang, M. H. Shaw, R. W. Evans and D. W. C. MacMillan, *Nat. Rev. Chem.*, 2017, 1, 0052.
- 5 E. M. Sherbrook, M. J. Genzink, B. Park, I. A. Guzei, M.-H. Baik and T. P. Yoon, *Nat. Commun.*, 2021, 12, 5735.
- 6 K. L. Skubi, T. R. Blum and T. P. Yoon, Chem. Rev., 2016, 116, 10035.
- 7 J. S. Trimble, R. Crawshaw, F. J. Hardy, C. W. Levy, M. J. B. Brown, D. E. Fuerst, D. J. Heyes, R. Obexer and A. P. Green, *Nature*, 2022, 611, 709.
- 8 N. Sun, J. Huang, J. Qian, T. Zhou, J. Guo, L. Tang, W. Zhang, Y. Deng, W. Zhao, G. Wu, R. Liao, X. Chen, F. Zhong and Y. Wu, *Nature*, 2022, 611, 715.
- 9 Y. Gu, K. Ellis-Guardiola, P. Srivastava and J. C. Lewis, *ChemBioChem*, 2015, **16**, 1880.
- 10 S. G. Keller, A. Pannwitz, F. Schwizer, J. Klehr, O. S. Wenger and T. R. Ward, *Org. Biomol. Chem.*, 2016, **14**, 7197.
- 11 G. Roelfes, Acc. Chem. Res., 2019, 52, 545.
- 12 S. H. Mejías, G. Roelfes and W. R. Browne, *Phys. Chem. Chem. Phys.*, 2020, **22**, 12228.
- 13 T. Kuckhoff, R. C. Brewster, C. T. J. Ferguson and A. G. Jarvis, *Eur. J. Org. Chem.*, 2023, e202201412.
- 14 Y. S. Zubi, B. Liu, Y. Gu, D. Sahoo and J. C. Lewis, *Chem. Sci.*, 2022, **13**, 1459.
- F. Schwizer, Y. Okamoto, T. Heinisch, Y. Gu,
 M. M. Pellizzoni, V. Lebrun, R. Reuter, V. Kohler,
 J. C. Lewis and T. R. Ward, *Chem. Rev.*, 2018, 118, 142.
- 16 E. H. Edwards and K. L. Bren, *Biotechnol. Appl. Biochem.*, 2020, **67**, 463.
- 17 Y. You and W. Nam, Chem. Soc. Rev., 2012, 41, 7061.
- 18 H. Yang, P. Srivastava, C. Zhang and J. C. Lewis, *ChemBioChem*, 2014, 15, 223.

19 B. Liu, L. Lystrom, C. G. Cameron, S. Kilina, S. A. McFarland and W. Sun, Eur. J. Inorg. Chem., 2019,

Communication

- 2019, 2208.
- 20 H. Yang, A. M. Swartz, H. J. Park, P. Srivastava, K. Ellis-Guardiola, D. M. Upp, G. Lee, K. Belsare, Y. Gu, C. Zhang, R. E. Moellering and J. C. Lewis, Nat. Chem., 2018, 10, 318.
- 21 B. Liu, L. Lystrom, S. Kilina and W. Sun, Inorg. Chem., 2019, 58, 476.
- 22 B. Liu, L. Lystrom, S. Kilina and W. Sun, Inorg. Chem., 2017, 56, 5361.
- 23 B. Liu, L. Lystrom, S. L. Brown, E. K. Hobbie, S. Kilina and W. Sun, Inorg. Chem., 2019, 58, 5483.
- 24 P. Haquette, J. Jacques, S. Dagorne, C. Fosse and M. Salmain, Eur. J. Inorg. Chem., 2010, 5087.
- 25 P. Srivastava, H. Yang, K. Ellis-Guardiola and J. C. Lewis, Nat. Commun., 2015, 6, 7789.

- 26 R. D. Gillard, in Progress in Inorganic Chemistry, ed. F. A. Cotton, John Wiley & Sons Inc., New York, 1st edn, 1966, vol. 7, ch. 4, p. 215.
- 27 L. Quintanar and L. Rivillas-Acevedo, Methods Mol. Biol., 2013, 1008, 267.
- 28 D. Rea and V. Fulop, Cell Biochem. Biophys., 2006, 44, 349.
- 29 K. Ellis-Guardiola, H. Rui, R. L. Beckner, P. Srivastava, N. Sukumar, B. Roux and J. C. Lewis, Biochem, 2019, 58, 1616.
- 30 J. C. Lewis, Acc. Chem. Res., 2019, 52, 576.
- 31 J. Lawandi, S. Gerber-Lemaire, L. Juillerat-Jeanneret and N. Moitessier, J. Med. Chem., 2010, 53, 3423.
- 32 E. M. Sherbrook, H. Jung, D. Cho, M. H. Baik and T. P. Yoon, Chem. Sci., 2020, 11, 856.
- 33 K. L. Skubi, J. B. Kidd, H. Jung, I. A. Guzei, M. H. Baik and T. P. Yoon, J. Am. Chem. Soc., 2017, 139, 171.